Flow Around Curved Tandem Cylinders

Tale E. Aasland*
Dept. of Marine Technology
The Norwegian University of Science and Technology
Trondheim, NO-7491
Norway
Email: tale.e.aasland@ntnu.no

Bjørnar Pettersen
Dept. of Marine Technology
The Norwegian University of Science and Technology
Trondheim, NO-7491
Norway

Helge I. Andersson
Dept. of Energy and Process Engineering
The Norwegian University of Science and Technology
Trondheim, NO-7491
Norway

Fengjian Jiang
Dept. of Ships and Ocean Structures
SINTEF Ocean
Trondheim, NO-7052
Norway

ABSTRACT

The flow around curved tandem cylinders of equal diameter has been investigated for the first time, by means of direct numerical simulations. A convex configuration was used.The nominal gap ratio was L/D = 3.0 and a Reynolds number of 500 was chosen. Due to the change in effective gap ratio along the cylinder axis, there is a variation of tandem flow regimes, from alternating overshoot/reattachment, via stable reattachment, to co-shedding, in this case called gap shedding. The combination of reattachment and gap

*Address all correspondence to this author.

shedding gives near-zero drag and vertical forces for the downstream cylinder, whereas the corresponding forces on the upstream cylinder are comparable to single curved cylinders. Meanwhile, the opposite is true for the lift forces. A low-frequency variation of horizontal and vertical forces is seen, and this is attributed to a slow variation of the position where gap shedding commences. Finally, the concept of a critical angle is proposed to describe the transition to gap shedding, for a given combination of nominal gap ratio and Reynolds number.

INTRODUCTION

Curved cylinders are of key interest in offshore applications, in particular when it comes to risers and pipelines. For single curved cylinders, the flow is highly dependent on the inflow direction with respect to the plane of curvature, as shown in several studies [1–5]. Directing the incoming flow towards the outer face of the cylinder (convex configuration) results in a completely different flow topology than directing it towards the inner face (concave configuration). The concave configuration has been studied by several [4,6–9], and the effect of oblique inflow angles was the subject of a recent study [5]. Vortex induced vibration of curved cylinders, an important engineering topic, has also been the subject of a number of studies in recent years [10–13]. As the current investigation is concerned with tandem curved cylinders in the parallel, convex configuration, we shall limit ourselves to describing the main contributions related to convex curved cylinders.

A pioneering work investigated flow around a cylinder at Reynolds numbers ($Re = U_0D/\nu$, where ν is the kinematic viscosity, D is the cylinder diameter, and U_0 is the free-stream velocity) 100 and 500 [2–4], by means of numerical simulations. The geometry consisted of a quarter-segment of a ring, with a radius of curvature of $r_c = 12.5D$. A horizontal extension of $L_h = 10D$ was used in the wake, but there was no vertical extension. An important result from this study was that there is a single vortex shedding-frequency along the entire cylinder, driven by the shedding at the top part, which is nearly normal to the incoming flow. This discovery challenges the so-called independence principle, where it is assumed that two-dimensional sections of a curved cylinder can be analyzed independently. Using this method, the shedding frequency would have varied along the span, according to the variation in local Reynolds number. Due to the axial curvature, there were strong vertical flow components, and it was estimated that approximately one third of the incoming flow rate was deflected downwards [4].

Later, the Reyndolds number was extended to the subcritical range [14–17], with $Re = 3900$. Direct numerical simulations (DNS) were used. The initial study [14] employed the same geometry as [4]. It was later discovered that the free-slip condition on the top boundary of the computational domain suppressed the vertical velocity component, unless a straight vertical extension $L_v = 6D$ was added to the geometry [15]. Because the vortex shedding frequency of the curved cylinder differed from that of the straight vertical extension, splitting of the spanwise vortices occurred near the interface between the two parts [16]. This manifested itself in a low-frequency variation of the velocity time traces, and was confirmed visually in the velocity field plots.

An experimental study investigated the effect of radius of curvature [6]. It was found that r_c impacts the Strouhal number ($St = fD/U_0$, where f is the vortex shedding frequency) , as well as the shedding angle of the spanwise vortices, but the influence decreases with increasing Reynolds number.

It is a challenge for the present study that there are few experimental investigations of single curved cylinders available in the literature. However, DNS is widely considered a high-fidelity method, and several of the aforementioned investigations use well-resolved DNS. Nonetheless, experimental results would be beneficial to further advance this field of research, and will hopefully be carried out in the future.

Flow around straight tandem cylinders is governed by the Reynolds number and the spacing between the cylinders , called the gap ratio. For tandem cylinders of equal diameter, the gap ratio is defined as L/D where *L* is the center-to-center distance. As the gap ratio is increased, the flow regime develops from overshoot, where the shear layers from the upstream cylinder bypass the downstream cylinder and roll up in the wake, through alternating and steady reattachment of the upstream shear layers onto the downstream cylinder, to co-shedding, where large-scale vortices are shed from both cylinders. The spacing at which co-shedding starts is called the critical spacing, L_c. It is well known that the transition from one tandem regime to another is strongly dependent on the Reynolds number [18], which makes it challenging to predict the exact gap ratio at which transition will occur. Nonetheless, the following classification is conventionally adopted: Overshoot $1.0 \leq L/D \leq 1.2-1.8$, reattachment $1.2-1.8 \leq L/D \leq 3.4-3.8$, and co-shedding $3.4-3.8 \leq L/D$ [19]. Within the reattachment regime, there is suction in the gap, so that the downstream cylinder experiences thrust instead of drag [20]. For this reason, the critical spacing is sometimes called the drag-inversion spacing, i.e. the spacing at which the downstream cylinder drag coefficient switches sign.

Thus far, there is only one study on the subject of two curved cylinders [21]. A side-by-side, convex configuration is used, with a Reynolds number of 500. To the knowledge of the authors, there are no studies that deal with tandem curved cylinders. However, a study of a symmetrically curved circular cylinder with variable span ratio (G/r_c where $G4$ is the distance between the cylinder ends) shares similarities with tandem cylinders when the span ratio is small [22]. The Reynolds number used was 100. An interesting result from that study is that the axial flow along the curved surface is influenced by the wake interference effects. While the side-by-side scenario is perhaps more common in the offshore industry, tandem configurations occur, and any challenges related to these must be clarified.

COMPUTATIONAL ASPECTS

Numerical method

In the present study, the full Navier-Stokes equations for incompressible flow are solved through DNS.

$$\frac{\partial u_j}{\partial x_j} = 0, \tag{1}$$

$$\frac{\partial u_i}{\partial t} + u_j \frac{\partial u_i}{\partial x_j} = -\frac{1}{\rho}\frac{\partial P}{\partial x_i} + \frac{\partial}{\partial x_j}\left(\nu\left[\frac{\partial u_i}{\partial x_j} + \frac{\partial u_j}{\partial x_i}\right]\right), i, j = 1, 2, 3 \tag{2}$$

All simulations were carried out using the MGLET flow solver. MGLET is based on a finite volume formulation of the incompressible Navier-Stokes equations, and uses a staggered Cartesian grid [23]. Solid bodies are introduced through an immersed boundary method [24], where the boundary is discretized using a cut-cell approach. A third-order low-storage explicit Runge-Kutta time integration scheme is used for time stepping, and the Poisson equation is solved using an iterative, strongly implicit procedure (SIP). MGLET has previously been used for convex [16] and concave [8, 9] curved cylinder studies.

Free-slip boundary conditions are used on all domain boundaries except the inlet and outlet. Uniform inflow is imposed at the inlet, and a Neumann condition is imposed on the velocity components at the outlet.

Computational domain, geometry and definitions

In the present study, the geometry consists of two curved tandem cylinders of equal diameter, with the plane of curvature parallel to the uniform inflow. The convex configuration is used, and the gap ratio is $L/D = 3.0$. The Reynolds number is 500, and this combination of gap ratio and Reynolds number is expected to fall under the reattachment regime for straight tandem cylinders. A Reynolds number of 500 is low for engineering purposes. However, given the novelty of this investigation, it is important to develop a thorough understanding of the basic flow physics before embarking on the more complex case of higher Reynolds numbers. Moreover, it allows more cases to compare with, as $Re = 500$ is used by several single curved cylinder studies.

The computational domain and geometry are depicted in figure 1a. The total domain size is $L_x \times L_y \times L_z = 43D \times 20D \times 33D$.

The curved part of the cylinder is a quarter-segment of ring with a radius of curvature r_c. The upstream cylinder has a radius of curvature of $r_{cu} = 12.5D$. In order to ensure a constant gap ratio along the entire geometry, a stronger curvature of $r_{cd} = 9.5D$ is used for the downstream cylinder. However, one of the challenges of a curved tandem cylinder setup is that, regardless of the inflow direction, the effective gap ratio will vary along the curved part of the cylinders. This is because the inflow cannot be normal to the local curvature at every point along the cylinder axis. Along the straight vertical extensions, the gap ratio is constantly $L/D = 3.0$, but along the curved part it increases with β. In accordance with previous results for a single curved cylinder [15], the curved tandem cylinders were fitted with straight vertical extensions of $L_v = 7D$, as well as horizontal extensions of $L_h = 15D$, in order avoid influence of the computational domain boundaries.

Herein, the x direction is referred to as streamwise and y direction as crossflow. The z direction is referred to as vertical, and vortical structures that align with this direction are dubbed spanwise. The time-averaged base pressure coefficient is given as $\overline{C}_{pb} = \overline{P} - \overline{P}_0/\overline{P}_s - \overline{P}_0$. Here, $\overline{P}_0$ is the free-stream pressure and $\overline{P}_s$ is the stagnation pressure. Force coefficients are defined as $\overline{C}_F = 2\overline{F}/\rho U_0 A$, where F is the force component in question, ρ is the fluid density and A is the projected frontal area. Subscripts D and L denote drag and lift, respectively, and subscript z denotes vertical force. Note that "lift" implies crossflow (i.e. y) direction in the present study. To separate the upstream and downstream cylinder coefficients, lower case u and d are used. The Strouhal numbers listed herein are based on spectral analysis of crossflow velocity time traces in the wake.

Grid independency and validation

Because there are no other tandem curved cylinder works to compare with, an initial study was carried out with two single curved cylinders of $r_c = 9.5D$ and $12.5D$. Four different grid were tested, but since this was merely used as a starting point for the tandem cylinder grid convergence study, only the results from the finest grid is shown herein. In table 1, the results are compared with the available literature. There is something of a spread in the values from different studies, but even so there is reasonable agreement with the present results.

A number of different grids were tested for the curved tandem cylinders, independently varying the refinement level on upstream and downstream cylinder, as well as in the gap. The flow is sensitive to the grid close to the upstream cylinder and in the gap region. This is no surprise, as these govern the inflow to the downstream cylinder, and hence are instrumental to the development of the wake. Refinement of the downstream cylinder influences its force coefficients, naturally, but also has some influence of the fluctuating lift of the upstream cylinder, through the interaction between the gap and wake flow.

Results for the four main grids are given in table 2. Here, all grids have equal element size on the upstream and downstream cylinders. For grids t1 and t2, the element size was the same for the cylinders and the gap region. For t3, the element size in the gap was twice that of the cylinder surface. For t4, the curved part of the gap was refined to the same element size as the cylinder surface. The remainder of the gap of t4 had grid cells twice that size, as illustrated in figure 1b.

The fluctuating lift and vertical forces, as well as the downstream cylinder drag coefficient, are most sensitive to grid refinement. There is a monotonic decrease of the upstream cylinder drag coefficient as the element size near the surface of the solid bodies is decreased. In addition, refinement of the gap region (from grid t3 to grid t4), further decreases the drag. However, the change in C_{Du} from the coarsest to the finest grid resolution is a mere 1.9 percent. The change in C_{Lrms} for the upstream and downstream cylinder from t2 to t4 is in the order of 2.0 percent. Figure 2 shows the effect of grid resolution on the time-averaged velocity field. The differences are in the order of 5 - 10 percent maximum if each of the profiles from grid t1 to t3 are compared with that of grid t4. With this in mind, the resolution of t2 may have been sufficient. Large differences between grids in the downstream cylinder drag, however, indicated that further refinement was needed.

The grid convergence study was complicated by the fact that there is long term variation of drag and vertical forces for both cylinders. For t1 and t2, statistics were sampled for 290 time units, tU_0/D, which correspond to approximately 40 vortex shedding cycles. Sampling started after 60 time units. For straight circular cylinder statistics, 40 cycles is ample, but in the present study, a longer sampling time is required. Therefore, statistics were sampled for 550 time units for t3, and 710 time units for t4, which amounts to approximately 81 and 106 large-scale vortex shedding cycles, respectively. In all simulations, the time step was adjusted by means of a built-in procedure in MGLET, in order to reach a target Courant number of 0.8. For t3 and t4, time step adjustment was carried out for 250 time units, after which sampling of statistics commenced.

In the end, grid t4 was chosen, due to the strong gradients in the curved gap region. The total number of elements was 529 million, and while this may seem excessive for a Reynolds number of 500, there is certainly enough uncharted territory in the present study to warrant careful treatment.

RESULTS

Flow topology

The instantaneous flow field is depicted in figure 3. We see that, similar to a single curved cylinder at this Reynolds number, there is shedding of slightly backwards-slanted, large-scale vortices in the wake. This is reminiscent of the flow topology in the wake of a yawed circular cylinder [25]. Because the effective gap ratio varies along the span of the cylinders, there is a variation of tandem flow regimes, from alternating overshoot/reattachment along the straight the vertical extensions, via stable reattachment in the upper part of the curved gap, to gap shedding, the equivalent of co-shedding, in the lower curved part. The approximate extent of the instantaneous reattachment zone is marked in figure 3a.

Due to the axial curvature, the flow is highly three-dimensional. At a Reynolds number of 500, the flow is expected to display a mode B instability of the wake [26], with streamwise structures of spanwise wavelength $\lambda \approx 1D$ bridging the von Kármán vortices. Evidence of this type of organization is seen throughout the instantaneous flowfield in figure 3b. However, the presence of the downstream cylinder, with some contribution from the gap shedding, causes bending and tilting of the vortices, so that a much more complex picture emerges.

The time-averaged streamwise and vertical velocity fields are shown in figures 4a and b, respectively. Recirculation zones, characterized by negative streamwise velocity, are clearly seen in figure 4a. These encompass the entire straight vertical gap and near wake, as well as approximately half of the curved part. Gap shedding, defined as $U/U_0 \leq 0$ at the front face of the downstream cylinder, commences at $\beta \approx 34.3°$.

The vertical velocity plot in figure 4b shows that there is a strong downdraft induced by the cylinder curvature. However, there are also zones of upwelling in the gap and near wake. Upwelling in the near wake is previously reported for a single curved cylinder, with a maximum velocity of $0.08U_0$ [16]. In the present study, the maximum upwelling velocity is approximately $0.093U_0$. Moreover, relatively high values of upwelling seem to occur along a larger portion of the vertical extension than for a single curved cylinder.

The strongest vertical flow occurs along the stagnation face of the upstream cylinder (see figure 4b), where the downdraft reaches $-0.44U_0$. However, the values in the gap are also quite significant. The maximum downdraft at the downstream cylinder stagnation face is $-0.37U_0$.

Previous studies of single curved cylinders have found that the axial flow suppresses vortex formation in the near wake, below $\beta \approx 45°$. A similar result is seen for the downstream cylinder, marked both in figure 3a and 4a. Recirculation in the wake, defined as $U/U_0 \leq 0$ along the back face of the downstream cylinder, is suppressed at approximately $36°$.

Because the axial velocity at the back face of the upstream cylinder is smaller than for the downstream cylinder (shown indirectly by the vertical velocity plot in figure 4b), it does not suppress the gap vortex shedding. In fact, gap shedding commences approximately in the region where recirculation is suppressed on the downstream cylinder. Meanwhile, the axial flow influences the orientation of the vortical structures. The gap vortices start out closely aligned with the cylinder curvature and the axial velocity, and appear to rotate so that they become almost normal to the axial velocity in the horizontal part of the gap, corresponding to the large-scale spanwise vortices in the wake. Figure 3 indicates that the gap shedding is in phase with the large-scale wake shedding.

Forces and frequencies

The forces experienced by the two cylinders are strikingly different from each other. As shown in table 3, the drag forces on the upstream cylinder are significantly larger than on the downstream cylinder. Moreover, the downstream cylinder experiences negative drag, i.e. a thrust force, albeit very small. This is consistent with the reattachment regime of straight tandem cylinders, where, we recall, recirculation in the gap causes a negative $\overline{C}_{Dd}$. If we separate the pressure forces and viscous forces, we see that they are similar in magnitude, with $\overline{C}_{Ddp} \approx -0.088$ and $\overline{C}_{Ddv} \approx 0.077$. In the current study, we have not quantified the force contributions from the straight extensions, but it is a likely hypothesis that the horizontal extension is responsible for the majority of the viscous drag. Conversely, there is recirculation along the entire gap between the straight vertical cylinders, as well as along nearly half of the curved gap, which results in negative pressure drag.

The main statistics for the curved tandem cylinder case show reasonable agreement with their straight counterparts in some parameters, shown in table 3. Note that the base pressure coefficients , as well as the separation and reattachment angles, are computed as the z direction average along the straight vertical extension, for the present study. This is to better facilitate comparison with straight tandem cylinders, since the values along the curved part vary considerably with the local curvature.

The upstream drag coefficient compares well with previous studies, although perhaps best with $Re = 1000$. The same is true for the fluctuating lift. The Strouhal number does not depart significantly from the value expected for straight tandem cylinders. For tandem cylinders, St is identical for the upstream and downstream cylinders, due to a "lock-in" effect [18]. This proves to be the case for curved tandem cylinders as well, although, as will be addressed in the discussion, there are small differences between the lower gap and the rest of the flow. The separation and reattachment angles, based on the zero shear stress criterion, also compare reasonably well, though there are few studies that provide this data.

The downstream force coefficients differ substantially from straight tandem cylinders. The reason for the discrepancy is twofold. Firstly, there is a significant positive contribution to the drag from the horizontal extensions, as well as from the part of the curved cylinder where there is gap shedding. These nearly balance the negative pressure drag from the reattachment region. All other studies in table 3 fall within the reattachment regime, and thus have negative C_{Dd}. Secondly, the vortex shedding strength of the downstream curved cylinder is weakened by the axial flow, causing smaller fluctuating lift, and possibly influencing the drag as well.

The value of the net vertical force is $\overline{C}_{zu} = 0.1854$ and $\overline{C}_{zd} = -0.0293$ for the upstream and downstream cylinder, respectively. $\overline{C}_{zu}$ corresponds well with single curved cylinder results, as shown in table 1, although it is somewhat smaller in magnitude. At first glance, the observation that $\overline{C}_{zd}$ should be negative appears somewhat peculiar. For a single curved cylinder, we assume that there are two main factors that ensure a positive net vertical force: backwards slanted spanwise vortices that give a vertical component, and the upwelling in the near wake. However, the upwelling velocities are very small and contribute primarily to the viscous forces. Thus, their contribution is expected to be nearly negligible. The negative vertical force component is mainly created by the induced downdraft.

For the curved tandem cylinders, in the part of the gap that falls under the reattachment regime, there is formation of quasi-steady vortices, similar to those reported by previous straight tandem cylinder studies [27–29]. These, as well as the shed gap vortices, align with the axial curvature of the cylinders, giving a net vertical force in the curved part of the gap. From figure 4c, we see that the vortices create a suction zone in the lower part of the gap, whose magnitude and extent are larger than those of the suction zone in the wake. The resulting pressure gradient contributes to a positive vertical force for the upstream cylinder, and a negative vertical force for the downstream cylinder.

The lift force on the upstream cylinder is very low compared to that on the downstream cylinder. In figure 5a, it is difficult to discern the large-scale wake shedding frequency, f_v, from other peaks, due to its low energy. This is probably due to the low energy of the quasi-steady gap vortices.

A portion of the upstream drag coefficient time trace is shown in figure 6a. There are low-frequency undulations in the drag forces, with a period of some 60 time units. The same type of time variation is visible in the downstream drag, in figure 6b, as well the vertical forces of both cylinders (not shown). The undulations are in-phase for the cylinders. In a previous study, low-frequency variation of the forces was related to the splitting and merging of spanwise vortices in the wake [16], which resulted in two dominant vortex shedding frequencies. Two dominant frequencies are not found in the present study, although spanwise vortex dislocations do occur quite frequently, as shown in figure 6c. However, there appears to be no obvious connection between these and the low-frequency undulations in the drag coefficient. A possible explanation is a low-frequency variation of the location of gap shedding inception. For straight tandem cylinders, co-shedding is associated with larger drag for the upstream cylinder and positive drag coefficient for the downstream cylinder. An upwards movement of the gap vortex shedding, with a corresponding shortening of the reattachment range, would intuitively cause a surge in drag for both cylinders.

DISCUSSION

The critical spacing is somewhat hard to define for this geometry, as both the effective gap ratio and the cross-sectional geometry changes with the curvature. In any given z/D plane along the curved section, the cross-sectional geometry is no longer cylindrical, but elliptical, with different streamwise lengths for the upstream and downstream cylinder. This implies that the classical definition of the gap ratio is no longer sensible. It would perhaps be more fruitful to characterize the advent of gap-shedding/co-shedding by a critical angle, for a given Reynolds number and nominal gap ratio. For straight tandem cylinders, the critical gap ratio decreases with increasing Reynolds number. Given that the inflow is parallel to the straight horizontal extensions, the critical angle is expected to decrease as the Reynolds number increases.

For straight tandem cylinders, transition between reattachment and co-shedding is associated with bistable flow, where co-shedding occurs intermittently [27]. For a symmetrically curved cylinder, it was found that intermittent transition occurred for Re = 100, at spacing ratios corresponding to a gap ratio in the range $3.76 \leq L/D \leq 4.53$ [22]. It was suggested that the induced axial flow was the perturbation that caused the switch, which was associated with a non-dimensional frequency of 0.0061. With this in mind, and given that the flow varies from overshoot/reattachment to co-shedding, it seems logical that bi-stability may occur in the present study, although we have not observed this directly. For straight tandem cylinders, bi-stability manifests itself in a secondary peak in the velocity spectra, with a frequency close to the single cylinder St, for a given Reynolds number [18, 27]. Such a peak is not immediately apparent in the velocity spectra in the present study. However, in the curved part of the gap, the dominant frequency changes to 0.162. This frequency is also in evidence in the vertical velocity component spectra for probes in the straight part of the gap, as exemplified in figure 7b. It is likely that the gap shedding frequency is influenced by the quasi-steady gap vortices, which share St with the wake shedding. This would explain why the gap shedding does not jump to the St of a single curved cylinder, the way co-shedding causes a jump in St for straight tandem cylinders. We note that the spectra from the symmetrically curved cylinder study ([22]-figure 21) also lack a secondary peak, although bi-stability was confirmed visually.

There is a possibility that the low-frequency variation of the forces, which we have already attributed to a change in the position of the gap shedding, can be linked to the bi-stability phenomenon. In previous studies, two bi-stable modes were found for straight tandem cylinders: one of short duration, and one where the duration was "very long" [27]. The duration of the bi-stable flow patterns was seen to increase when the critical spacing was approached. This means that for straight tandem cylinders near the critical spacing, the secondary peak in the velocity spectra should have a magnitude close to that of the dominant peak. In the present study, the velocity time traces display the same low-frequency variation as the forces, and the surges in the force components are associated with surges in vertical gap velocities as high up as $z/D = 2.0$ (see figure 7a). Spectra of the vertical component do display a secondary peak near $fU_0/D = 0.162$, which increases in magnitude as we move further into the curved gap. This supports the hypothesis that the low-frequency variation is related to bi-stability.

Despite the $7D$ vertical extension, there is some influence from the top boundary, which is visible as an unphysical bump in the $U/U_0 = 0$ contour in the upper part of figure 4a. This indicates that further studies of curved tandem cylinders require an investigation into the effect of the vertical extension length.

SUMMARY AND CONCLUSIONS

The flow around curved tandem cylinders has been investigated for the first time, using DNS. The inflow was parallel to the plane of curvature, and the convex configuration was chosen. The Reynolds number was 500. Similar to single curved cylinders, there are significant negative vertical velocities due to the curvature, and the wake is highly three-dimensional. The wake vortex shedding is in-phase along the span, with a slight backwards slanting of the vortex lines.

It was found that, due to the gradual change in effective gap ratio along the curved part of the cylinder, several tandem flow regimes co-exist in the flow. Along the straight vertical extension, there is alternating overshoot/reattachment, which changes to stable reattachment and, finally, gap shedding in the curved gap. Because recirculation is suppressed for the downstream cylinder in the region where vortices are shed from the upstream cylinder, the term gap shedding is adopted instead of co-shedding, which would be inaccurate.

Due to reattachment, there is suction in a large portion of the gap, which leads to a state of near-zero drag for the downstream cylinder. Conversely, the lift forces on the upstream cylinder are very small, due to the weakness of the quasi-steady gap vortices.

There is a significant positive vertical force on the upstream cylinder, which is comparable to the values for single curved cylinders at the same Reynolds numbers. Meanwhile, the downstream cylinder experiences very small, but negative, vertical forces. This is because positive contributions to the vertical forces by the slanted wake vortices are balanced by the negative contribution from the vortices in the gap, as well as downdraft induced by the axial curvature.

Because the effective gap ratio, and hence the tandem flow regime, varies along the cylinder axis, we suggest that instead of using the term critical spacing to describe the transition to shedding in the gap, the concept of a critical angle should be used. Based on the behavior of straight tandem cylinder flow, the critical angle is expected to decrease with increasing Reynolds number, for a given nominal gap ratio.

A low-frequency variation of the drag and vertical force is observed, and this is attributed to a slow variation of the gap shedding inception angle. A smaller angle, resulting in shedding in a larger portion of the gap, is associated with increased drag for the upstream cylinder, and drag inversion for the downstream cylinder. We believe that this slow variation of the gap shedding is related to bi-stability of the flow near the critical angle.

ACKNOWLEDGEMENTS

We would like to thank the Research Council of Norway and The Norwegian Public Roads Administration for providing funding for this work. Computational hours were granted by the Norwegian HPC project NN9191K.

REFERENCES

[1] Ahmed, A., 2001. "Flow field of a curved cylinder". In 39th Aerospace Sciences Meeting and Exhibit, 08 - 11 Jan. 2001, Reno, NV, USA, American Inst. of Aeron. and Astron.

[2] Miliou, A., Sherwin, S. J., and Graham, J. M. R., 2003. "Fluid dynamic loading on curved riser pipes". *ASME J. Off. Mech. Arctic Eng.,* **18**(1), pp. 29–40.

[3] Miliou, A., Sherwin, S. J., and Graham, J. M. R., 2003. "Wake Topology of Curved Cylinders at Low Reynolds Numbers". *Flow, Turb. Comb.,* **71**, pp. 157–160.

[4] Miliou, A., De Vecchi, A., Sherwin, S. J., and Graham, J. M. R., 2007. "Wake dynamics of external flow past a curved cylinder with free stream aligned with the plane of curvature". *J. Fluid Mech.,* **592**, pp. 89–115.

[5] Lee, S., Paik, K.-J., and Srinil, N., 2020. "Wake dynamics of a 3D curved cylinder in oblique flows". *Int. J. Naval Arch. Ocean Eng.,* **12**, pp. 501–517.

[6] Shang, J. K., Stone, H. A., and Smits, A. J., 2018. "Flow past finite cylinders of constant curvature". *J. Fluid Mech.,* **837**, pp. 896–915.

[7] Jiang, F., Pettersen, B., Andersson, H. I., Kim, J., and Kim, S., 2018. "Wake behind a concave curved cylinder". *Phys. Rev. Fluids,* **3**, p. 094804.

[8] Jiang, F., Pettersen, B., and Andersson, H. I., 2018. "Influences of upstream extensions on flow around a curved cylinder". *Eur. J. Mech. / B Fluids,* **67**, pp. 79–86.

[9] Jiang, F., Pettersen, B., and Andersson, H. I., 2019. "Turbulent wake behind a concave curved cylinder". *J. Fluid Mech.,* **878**, pp. 663–699.

[10] de Vecchi, A., Sherwin, S. J., and Graham, J. M. R., 2008. "Wake dynamics of external flow past a curved circular cylinder with the free-stream aligned to the plane of curvature". *J. Fluids Struct.,* **24**, pp. 1262–270.

[11] Assi, G., Srinil, N., Freire, C., and Korkischko, I., 2014. "Experimental investigation of the flow-induced vibration of a curved cylinder in convex and concave configurations". *J. Fluids Struct.,* **44**, pp. 52–66.

[12] Seyed-Aghazadeh, B., Budz, C., and Modarres-Sadeghi, Y., 2015. "The influence of higher harmonic flow forces on the response of a curved circular cylinder undergoing vortex-induced vibration". *J. Sound Vib.,* **353**, pp. 395–406.

[13] Srinil, N., Ma, B., and Zhang, L., 2018. "Experimental investigation on in-plane/out-of-plane vortex-induced vibrations of curved cylinder in parallel and perpendicular flows". *J. Sound Vib.,* **421**, pp. 275–299.

[14] Gallardo, J. P., Pettersen, B., and Andersson, H. I., 2011. "Dynamics in the wake of a curved circular cylinder". In 13th European Turbulence Conference (ETC2013), Vol. 318 of *J. Physics: Conference Series*, p. 062008.

[15] Gallardo, J., Pettersen, B., and Andersson, H. I., 2013. "Effect of free-slip boundary conditions on the flow around a curved circular cylinder". *Computers and Fluids,* **86**, pp. 389–394.

[16] Gallardo, J., Andersson, H. I., and Pettersen, B., 2014. "Turbulent wake behind a curved circular cylinder". *J. Fluid Mech.,* **742**, pp. 192–229.

[17] Gallardo, J., Pettersen, B., and Andersson, H. I., 2014. "Coherence and Reynolds stresses in turbulent wake behind a curved circular cylinder". *J. Turbulence,* **15**, pp. 883–904.

[18] Xu, G., and Zhou, Y., 2004. "Strouhal numbers in the wake of two inline cylinders". *Exp. Fluids,* **37**, pp. 248–256.

[19] Zdravkovich, M. M., 1987. "The effect of interference between circular cylinders in cross flow". *J. Fluids Struct.,* **1**, pp. 239–261.

[20] Sumner, D., 2010. "Two circular cylinders in cross-flow: A review". *J. Fluids Struct.,* **26**, pp. 849–899.

[21] Gao, Y., He, J., Ong, M. C., Zhao, M., and Wang, L., 2021. "Three-dimensional numerical

investigation on flow past two side-by-side curved cylinders". *Ocean Eng.,* **234**, p. 109167.

[22] Zhu, H., Wang, R., Bao, Y., Zhou, D., Ping, H., Han, Z., and Sherwin, S. J., 2019. "Flow over a symmetrically curved circular cylinder with the free stream parallel to the plane of curvature at low Reynolds number". *J. Fluids Struct,* **87**, pp. 23–38.

[23] Manhart, M., 2004. "A zonal grid algorithm for DNS of turbulent boundary layers". *Computers and Fluids,* **33**, pp. 435–461.

[24] Peller, N., Le Duc, A., Tremblay, T., and Manhart, M., 2006. "High-order stable interpolations for immersed boundary methods". *Int. J. Num. Meth. Fluids,* **53**, pp. 1175–1193.

[25] Thakur, A., Liu, X., and Marshall, J. S., 2004. "Wake flow of single and multiple yawed cylinders". *ASME J. Fluids Eng.,* **126**, pp. 861–870.

[26] Williamson, C. H. K., 1996. "Vortex dynamics in the cylinder wake". *Annu. Rev. Fluid. Mech.,* **28**, pp. 477–539.

[27] Igarashi, T., 1981. "Characteristics of the flow around two circular cylinders arraged in tandem (1st report)". *Bull. JSME,* **24**(188), pp. 323–330.

[28] Lin, J.-C., Yang, Y., and Rockwell, D., 2002. "Flow past two cylinders in tandem: Instantaneous and averaged flow structure". *J. Fluids Struct.,* **16**(8), pp. 1059–1071.

[29] Kitagawa, T., and Ohta, H., 2008. "Numerical investigation on flow around circular cylinders in tandem arrangement at a subcritical Reynolds number". *J. Fluids Struct.,* **24**, pp. 680–699.

[30] Papaioannou, G., Yue, D. K. P., Triantafyllou, M., and Karniadakis, G. E., 2006. "Three-dimensionality effects in flow around two tandem cylinders". *J. Fluid Mech.,* **558**, pp. 387–413.

[31] Song, Y., and Zhu, R., 2017. "A numerical study of flow patterns, drag and lift for low Reynolds number flow past tandem cylinders of various shapes". In ASME 2017 Mech. Eng. Cong. and Expo. IMEC2017, p. 70089.

[32] Zhou, Q., Alam, M., Cao, S., Liao, H., and Li, M., 2019. "Numerical study of wake and aerodynamic forces on two tandem circular cylinders at Re 1000.". *Phys. Fluids,* **31**, p. 045103.

[33] Lee, T., and Basu, S., 1997. "Nonintrusive measurements of the boundary layer developing on a single and two cylinders". *Exp. Fluids,* **23**, pp. 187–192.

[34] Arie, M., Kiya, M., Mriya, M., and Mori, H., 1983. "Pressure fluactuations on the surface of two circular cylinders in tandem arrangment". *ASME J. Fluids Eng.,* **105**, pp. 161–167.

LIST OF FIGURES

LIST OF TABLES

FIGURES

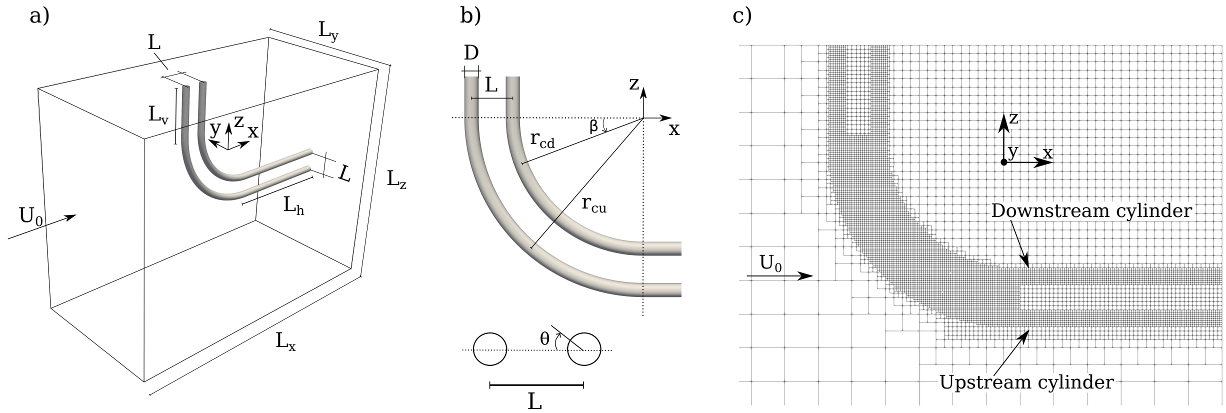

Fig. 1. a) Computational domain and geometry b) coordinate system and definitions c) schematic of the refinement regions of the computational grid. The origin is placed at the center of curvature of the cylinders.

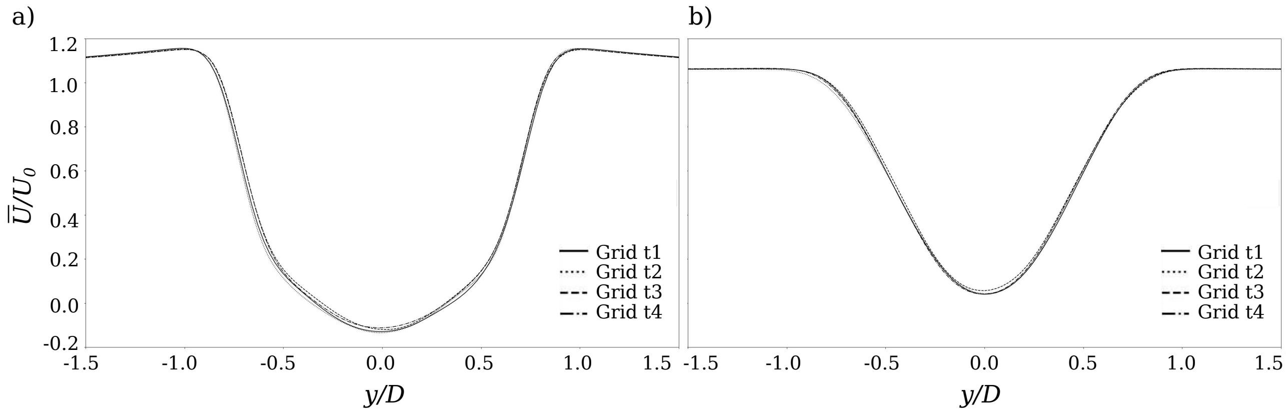

Fig. 2. Profiles of time-averaged streamwise velocity in the a) gap and b) wake, one diameter downstream of the upstream and downstream cylinder, respectively. Coordinates of the profiles are a) $(x/D = -11, z/D = 0)$ and b) $(x/D = -8.0, z/D = 0)$.

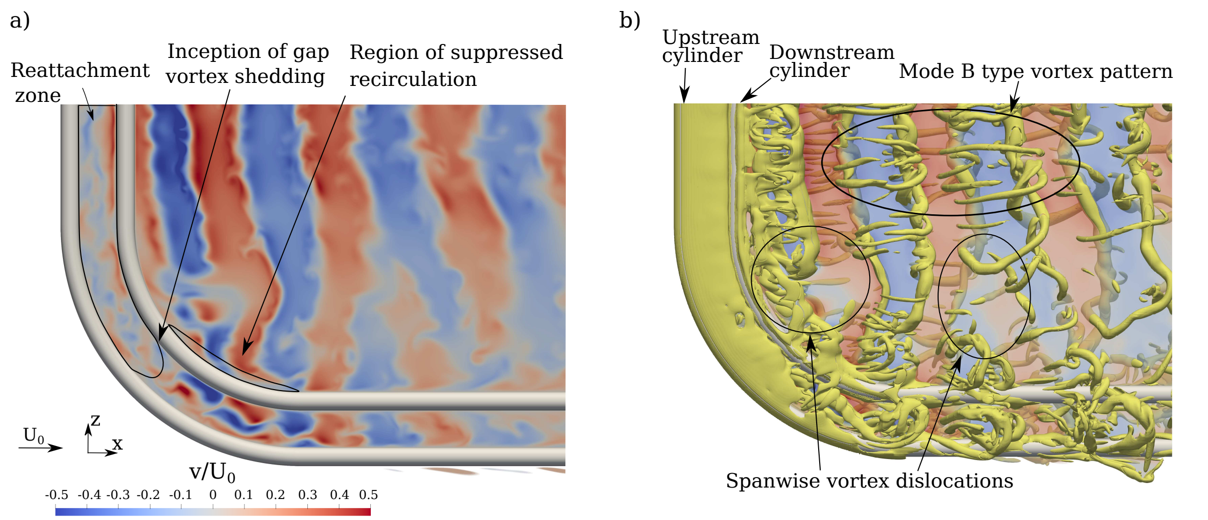

Fig. 3. a) Instantaneous crossflow velocity in the plane $y/D = 0$, at $tU_0/D = 800$, with b) isosurfaces of $Q(D/U_0)^2 = 0.1$ superimposed (yellow). Coordinate axis for orientation only.

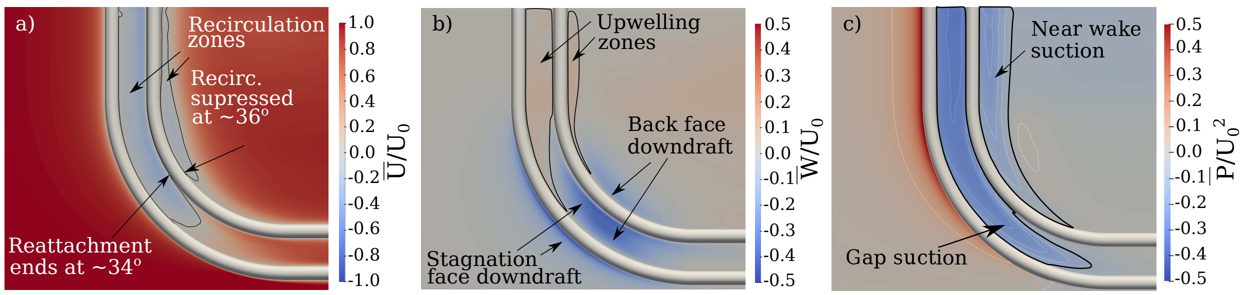

Fig. 4. Time-averaged flow field. a) streamwise and b) vertical velocities, and c) pressure.

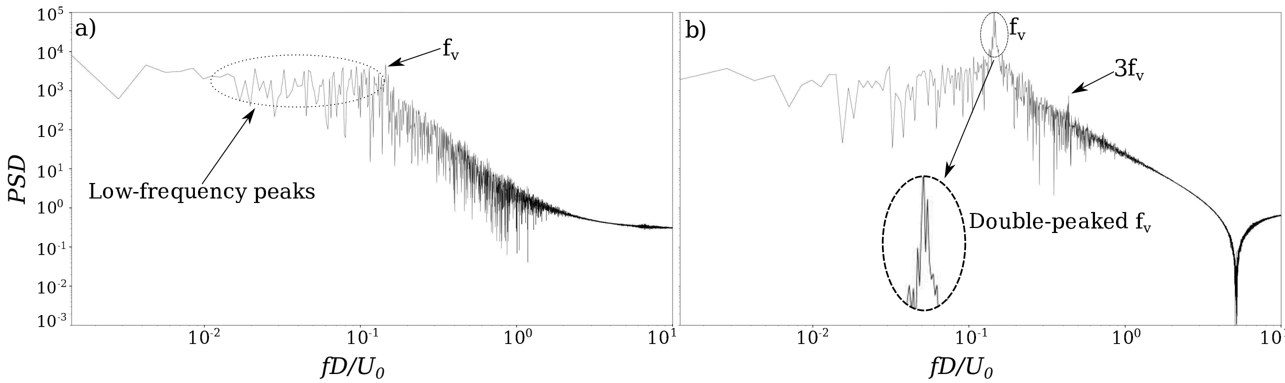

Fig. 5. Power spectral density (PSD) of crossflow forces for the a) upstream and b) downstream cylinder

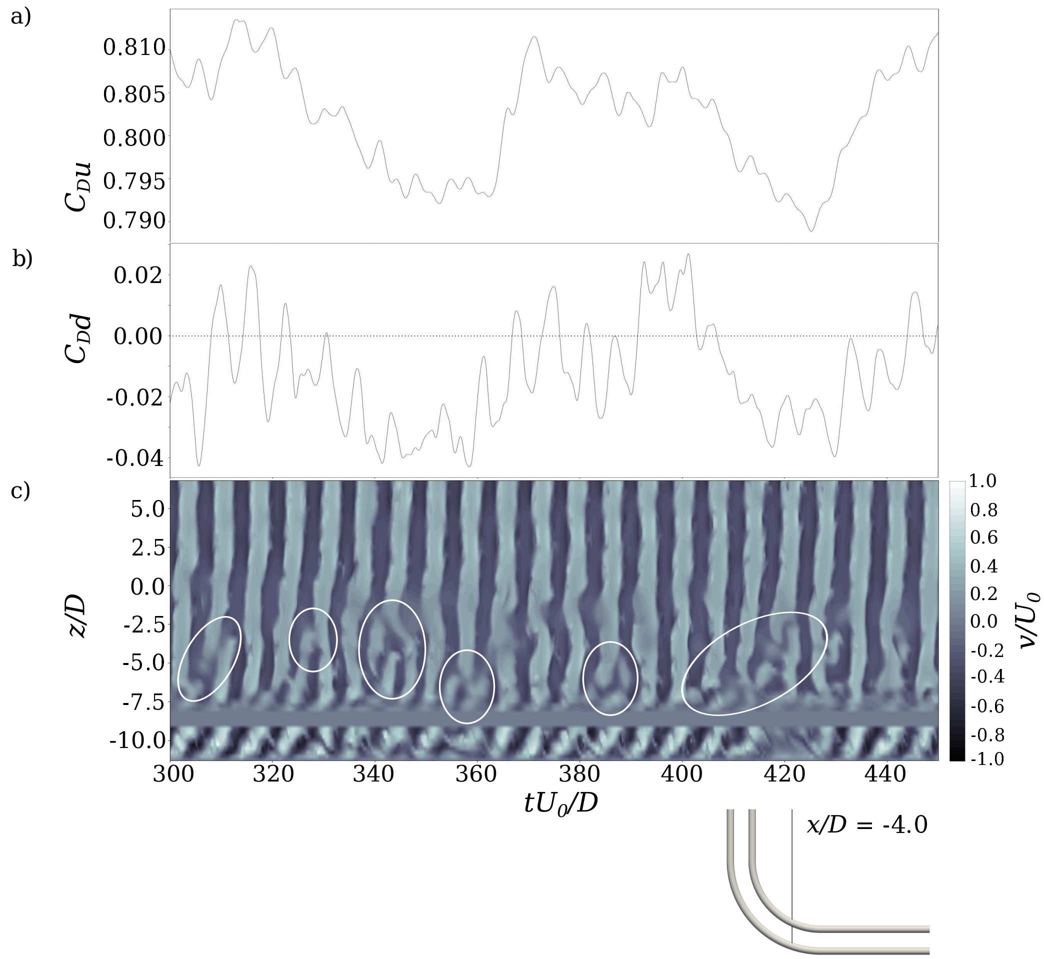

Fig. 6. a) Upstream and b) downstream drag coefficient time trace. Note that C_{Du} and C_{Dd} are not on the same scale. c) Time evolution of the spanwise crossflow velocity distribution in the wake, at $x/D = -4$. Vortex locations are marked by white rings. The downstream cylinders itself is visible as a straight horizontal band, and the location of the velocity probe line at $x/D = -4.0$ is shown in the bottom of the figure.

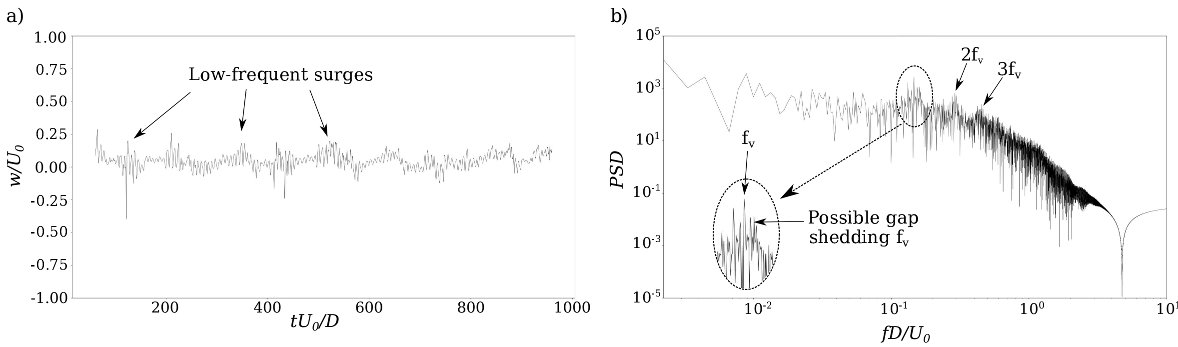

Fig. 7. a) vertical velocity time trace b) spectrum in the straight vertical gap, at $(x/D, y/D, z/D) = (-10.5, 0.65, 2.0)$

TABLES

	Δ_{min}/L	no. elem.	r_c/D	Re	$\overline{C}_D$	C_{Lrms}	$\overline{C}_z$	St	Method
r9.5	0.0125	99M	9.5	500	1.001	0.130	0.233	0.213	DNS
r12.5	0.0125	106M	12.5	500	1.001	0.149	0.247	0.208	
[21]*			12.5	500	1.310	0.549		0.204	DNS
[16]			12.5	3900	0.742	0.017	0.182	0.213/0.223	DNS
[5]			12.5	500	0.872		0.343		LES
[4]			12.5	500	0.92		0.380		
[6]			19.1	458				0.155	Exp.

Table 1. Results from the single curved cylinder grid study, compared with convex cases in the literature. M denotes million. *Data from a single curved cylinder validation case.

Grid	Δ_{min}/L	no. elem.	$\overline{C}_D$	C_{Lrms}	$\overline{C}_z$	St
			Upstream cylinder			
t1	0.015	104 M	0.8144	0.0192	0.1897	0.148
t2	0.0125	216 M	0.8079	0.0205	0.1830	0.152
t3	0.0075	364 M	0.8026	0.0180	0.1896	0.148
t4	0.0075	529 M	0.7995	0.0209	0.1854	0.152
			Downstream cylinder			
t1	0.015	104 M	-0.01359	0.1603	-0.0311	0.148
t2	0.0125	216 M	-0.0166	0.1561	-0.0304	0.152
t3	0.0075	364 M	-0.0113	0.1556	-0.0331	0.148
t4	0.0075	529 M	-0.0112	0.1545	-0.0293	0.152

Table 2. Main statistics from curved tandem cylinder grid study

	Upstream cylinder				Downstream cylinder					
	$\overline{C}_{Du}$	C_{Lrmsu}	$-\overline{C}_{pbu}$	θ_u [deg]	$\overline{C}_{Dd}$	C_{Lrmsd}	$-\overline{C}_{pbd}$	θ_d [deg]	θ_r [deg]	St
present study	0.7995	0.0209	0.69	98.05	-0.0112	0.1545	0.49	126.87	68.9	0.152
Straight tandem cyl. studies:										
$Re = 500$, $L/D = 2.5$ [30]	0.958				-0.142					0.150
$Re = 500$, $L/D = 3.5$ [30]	0.894				-0.126					0.144
$Re = 500$, $L/D = 3.0$ [18]										0.168
$Re = 500$, $L/D = 3.0$ [31]	1.12				-0.25					
$Re = 1000$, $L/D = 3.0$ [32]	0.88	0.03	0.63	92.5	-0.15	0.34	0.42	125	67	0.149
$Re = 2.2 \times 10^4$, $L/D = 3.0$ [29]	0.80	0.02	0.6		-0.20	0.3	0.4		70	0.155
$Re = 4.0 \times 10^4$, $L/D = 3.2$ [33]							0.45	120	67.2	0.144
$Re = 1.57 \times 10^5$, $L/D = 2.0$ [34]		0.1	0.9			0.7	0.6		60	
$Re = 1.57 \times 10^5$, $L/D = 3.0$ [34]		0.02	0.75			0.48	0.49		none	

Table 3. Main statistics for curved tandem cylinders compared with straight tandem cylinders from the literature. θ_u and θ_d denote the primary separation angle of the upstream and downstream cylinders, respectively, and θ_r denotes the reattachment angle.